Journal of Visualization, Vol. 1, No. 4 (1999) 355-364

Three-dimensional Temperature Measurement in Turbulent Thermal Convection by Extended Range Scanning Liquid Crystal Thermometry

Fujisawa, N.*[1, 2] and Adrian, R. J.*[1]

*1 Department of Theoretical and Applied Mechanics, University of Illinois, Urbana, Illinois 61801, USA.
*2 Research performed while on leave from Department of Mechanical System Engineering, Gunma University, Kiryu, 376, Japan (Present address: Department of Mechanical and Production Engineering, Niigata University, Niigata, 950-2181, Japan).

Received 30 October 1998.
Revised 12 February 1999.

***Abstract*:** The usable temperature range of liquid crystal thermometry has been extended and used to measure three-dimensional temperature fields in turbulent thermal convection. The color of the liquid crystals is calibrated against temperature using the standard method in which hue is the single input variable and two new methods: hue/intensity as input variable, and hue, saturation and intensity as input variables to a neural network. Relative to the hue calibration, the new methods extend the range over which temperature can be measured by more than 100%. Three-dimensional temperature measurements of turbulent thermal convection over smooth surfaces were carried out at a flux Rayleigh number of 3×10^9 by scanning a white light sheet normal to the visualized image plane and capturing a number of sequential images at various positions of the light sheet. Stacks of the planar data were composed into three-dimensional temperature distributions. The results indicate the presence of an irregular spoke pattern over the surface and the generation of plumes from the intersections of the patterns, consistent with other investigations.

***Keywords*:** thermometry, liquid crystal, three-dimensional, thermal convection.

1. Introduction

Numerous investigators (Rhee, et al., 1984 and others) have used liquid crystals, usually in microencapsulated form, to visualize the temperature field of thermal flow. When illuminated by white light the color of the light reflected by the liquid crystals changes with increasing temperature from colorless to red at low temperature, passes through green and blue to violet and turns colorless again at high temperature. Temperature visualization can be made quantitative by calibrating the color of the liquid crystal versus temperature using various approaches. Wilcox, et al. (1985) proposed a color photography technique, and Akino, et al. (1986) performed calibration of the wavelength of the color against temperature using a monochrome CCD camera and interference filters. The implementation of color CCD cameras is a natural step that has been applied to liquid crystal thermometry by relating their R-G-B outputs to the temperature of the suspended liquid crystals (*c.f.* Akino, et al., 1988 and Kimura, et al., 1989). Instead of calibrating temperature against location in R-G-B color space, Dabiri and Gharib (1991) proposed the use of hue-saturation-intensity (H-S-I) color space with hue as the single calibration variable. In other words, they showed that a usable relationship could be established between the hue and the temperature. Since then, the hue calibration technique has been applied successfully to several thermal phenomena by Ozawa, et

al. (1992), Nozaki, et al. (1995) and Kobayashi, et al. (1995). In a rather different approach, Kimura, et al. (1989) studied a neural network as a means to convert the three input variables from R-G-B color space into a single output variable. The parameters of the neural net were chosen so as to make the output variable correspond closely to the temperature. This approach is fairly general, and it permits calibration of temperature in situations where the hue calibration is not unique. Kasagi, et al. (1989) and Dabiri and Gharib (1991) provide additional details about the chemical and optical characteristics of liquid crystals.

The purpose of the present investigation is to extend the earlier planar light sheet studies of two-dimensional thermal plume structure (Keane and Adrian, 1995, Keane, et al., 1997) by performing quantitative measurements of the three-dimensional temperature field using liquid crystal thermometry with a scanning light sheet. The calibration of color as a function of temperature is performed by various techniques, and their respective calibration errors are examined. The three-dimensional temperature distributions of thermal convection over a smooth surface are measured, and the structures of the thermal plumes are discussed.

2. Experimental Apparatus and Procedures

2.1 Optical Characteristics of Liquid Crystals

The liquid crystals used in the present experiment were encapsulated chiral nematic particles of diameter 10-15 μm, which are provided by Hallcrest Co. in the form of a 33% solid slurry in water. It is known that the chiral nematic type of liquid crystal reflects a brighter color than the cholesteric type, and hence the chiral nematic type is better suited to flow visualization purposes (Hallcrest, 1996). The liquid crystals are named based on the red starting temperature and the color sensitive temperature range. We used two types, R32C2W and R29C4W, where the red starts at 32°C and 29°C with the temperature ranges of 2°C and 4°C, respectively. In the experiments, the slurries of liquid crystals were added to de-ionized water to form a very dilute suspension with a volume concentration of 0.004%. The temperature-color calibration was carried out using a test vessel having horizontal dimensions 148mm $\times$ 158mm and 100mm in height. The liquid was heated from the bottom boundary using an electric heater, and it was mixed well to create uniform temperature. A platinum thermometer measured the liquid temperature with an accuracy of 0.01°C, and a color CCD camera in R-G-B color space captured the visualized images. In order to minimize the color change due to the viewing angle, the color CCD camera was located 2m from the test vessel, and a telephoto lens was used (Ozawa et al., 1992) to reduce the viewing angle of the camera to less than 1.4°. The R-G-B outputs from the frame grabber were converted to H-S-I color space using Image Pro image processing software (Media Cybernetics). This software calculates the hue H by using a linear approximation inside a 60° color hexagon, where $H=[\pi/2 - \arctan\{(2R - G - B)/\sqrt{3}\,(G - B)\}+\pi;\ G<B]/2\pi$. In terms of the values of R, G and B, the intensity is $I = (R + G + B)/3$, and the saturation is $S=(I - \min(R, G, B))/I$. It was observed that the color of the liquid crystals degraded slowly with time, and that the liquid crystals with the smaller temperature range (R32C2W) were more susceptible to degradation. Therefore, the calibration measurements were carried out at a fixed time (1 hour) after preparing the water/liquid crystal mixtures.

2.2 Experimental Setup for Three-dimensional Temperature Measurements

Figure 1 shows the experimental set-up for measuring the three-dimensional temperature distribution of turbulent thermal convection. A slide projector setting on a traverse mechanism driven by a stepping motor produced a light sheet that moved in a direction normal to the plane of light sheet. The thickness of the light sheet, 2mm, was thin enough to resolve the structure of thermal plumes, which were approximately 200mm wide. The images obtained at the various cross sections were sequentially captured by the CCD camera and color frame grabber, and transferred to RAM memory in a personal computer. The resolution of each captured image was 512 $\times$ 480 with 8bits amplitude range for each component (R, G, B) of color. The distance between the CCD camera and the target image was set to 2m, as in the calibration. The light sheet was moved at a constant velocity of 7.2mm/sec, and the frame rate of the camera was set to 3.6frame/sec. Thus, a total of twenty-five sequential images spanning a 50mm wide domain was captured in 7sec. During this scanning time the fluid motion, of order 2mm/s $\times$ 7s~14mm caused non-negligible deformation of the plume structure. This is a technical difficulty that can be resolved in the future with faster frame rate data acquisition. For the present experiment, the skewing produced by the limited framing capability of our camera was tolerated. The liquid crystals respond to temperature changes with time constants of the order of milliseconds (Ozawa, 1992). This response was fast enough to follow the most rapidly evolving thermal structures in the present experiment.

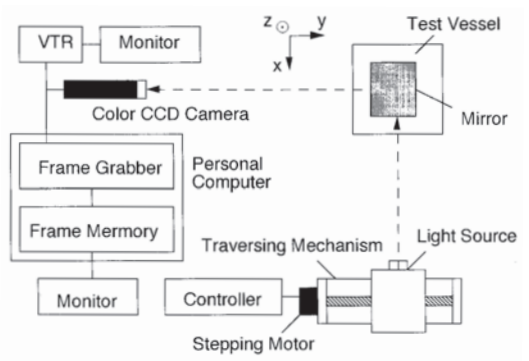

Fig. 1. Experimental setup for three-dimensional temperature measurement.

2.3 Thermal Convection Test Section

Figure 2 illustrates our experimental test section for turbulent thermal convection over smooth surfaces. It had a horizontal cross-sectional area of 508mm × 508mm, and it was 100mm high. The lower boundary, through which heat was conducted into the convective layer of water, was a 19mm thick aluminum plate heated from below by an electrical heating mat. Experiments were carried out at a flux Rayleigh number $Ra_f = \beta g Q h^4 / \nu^2 \kappa = 3 \times 10^9$ (β = thermal expansion coefficient of water, g = gravitational acceleration, Q = mean kinematic heat flux, h = height of fluid layer, κ = thermal diffusivity, ν = kinematic viscosity). The surrounding plates are made of 10mm thick Plexiglas, and the heat loss was minimized by enclosing the box in Styrofoam insulation, except for its top and front boundaries. Illumination entered through the top boundary using an inclined mirror located over the test section.

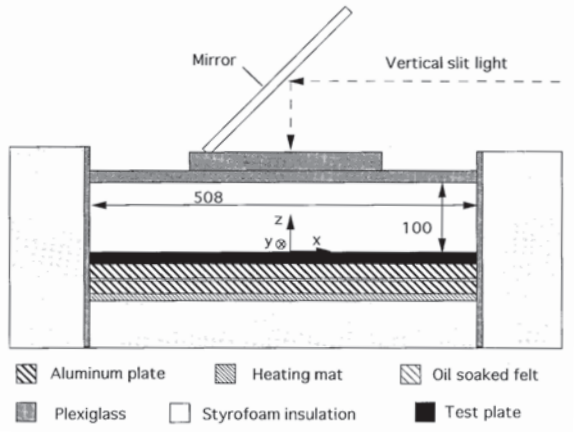

Fig. 2. Thermal convection test section.

3. Results and Discussions

3.1 Optical Characteristics and Calibration Techniques of Liquid Crystals

Figures 3 (a)-(c) give the measured hue H, saturation S and intensity I of the liquid crystals in relation to the measured temperature T_m. Values of H, S, and I range from 0 to 255. Each figure presents the results for the two liquid crystals R32C2W and R29C4W, which show similar variations with the temperature. Figure 3 (a) shows that the hue increases from red at low temperature to blue then green on a curve that is monotonic except in a small range at low temperatures. The temperature sensitivity, defined as the rate of change of hue with respect to temperature, is large around red and green, but decreases gradually as the hue increases to blue. It should be noted that the value of the hue at low temperature H=–70, corresponds to the hue at high temperature H=186, because hue is cyclic over the range 0~255. Also, there is a small temperature range, around 28-29°C in which hue is not monotonic, as mentioned by Kobayashi, et al. (1995) and others. In order to obtain a one-to-one correspondence

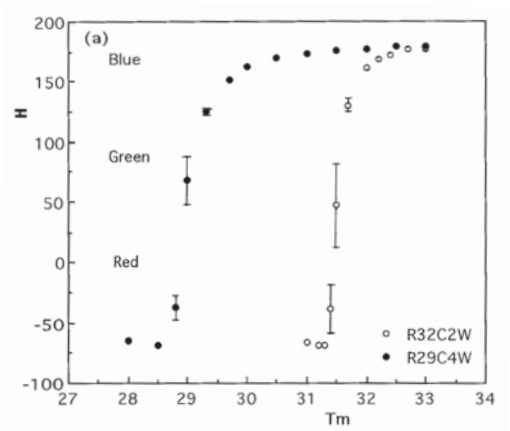

(a)

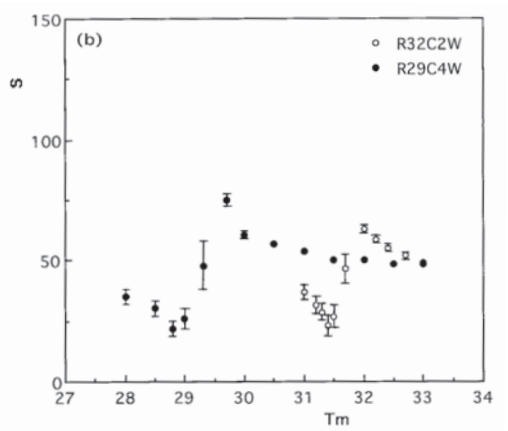

(b)

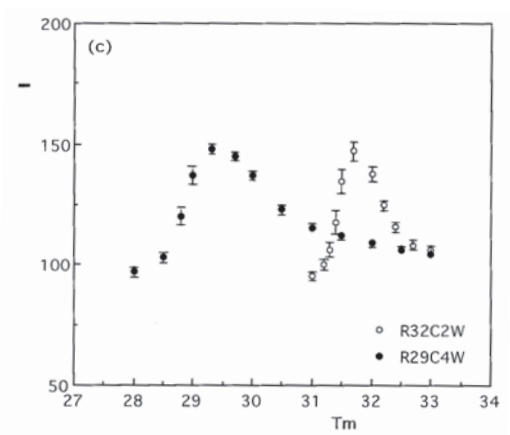

(c)

Fig. 3. Optical characteristics of liquid crystals in *H*-*S*-*I* color space.
(a) Hue *H*, (b) Saturation *S*, (c) Intensity *I*.

between hue and temperature, one can exclude this range from the calibration curve, as was done by Dabiri and Gharib (1991). But, this wastes much of the red range of color play, and results in a rather limited total temperature range.

The error bars in Fig. 3 indicate the scatter of the data obtained by repeated calibration experiments. It is clear that the error bar is largest near the red starting temperature, reflecting the higher sensitivity of the liquid crystals in this range.

Figure 3(b) shows the variation of the saturation with the temperature. For the R29C4W liquid crystal, the saturation *S* increases suddenly near the red starting temperature, and then stays relatively constant. The sensitivity of the saturation with respect to temperature is less than the sensitivity of the hue, so it is a less accurate measure of temperature than hue. But, saturation can be used to distinguish between low and high temperatures, when corresponding hue values are very close to each other, as in the case of the present liquid crystals. Figure 3(c) shows the intensity characteristics of the liquid crystals. They have a peak near the red starting temperature, and they decrease gradually on both sides of the temperature range. The intensity decreases gradually in the high temperature range, and it has even higher sensitivity to temperature than that of the hue. This suggests that using both hue and intensity as calibration parameters may provide a more accurate temperature calibration technique.

Figure 4 shows how the proposed new calibration variable H/I, depends upon temperature. The curve of H/I versus T_m has more uniform sensitivity to temperature than that of H versus T_m, and it generally improves the sensitivity to temperature over a somewhat wider temperature range. As H/I at low temperature is very close to that at high temperature (due to the cyclic nature of hue), calibration using H/I suffers from the same problem as the hue calibration. Suppose for the sake of discussion that we rescale H and H/I to make them equal to 0 at the start of the red and 255 at the end of the blue. Small errors in the measurement of H/I at the high temperature end of the range, where H~255, could yield values somewhat greater than 255, corresponding to H~0; this would

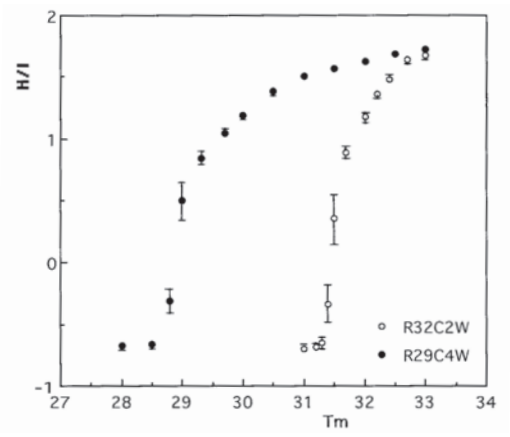

Fig. 4. *H*/*I* versus temperature.

spuriously indicate a temperature at the low end of the range. A simple means of eliminating this problem is to associate all measurements whose values for saturation lie between 0 and a threshold value S_c with the low temperature range. All measurements whose saturation lies above S_c are associated with the high temperature range. A good value of S_c is found to be 45 in the present experiment. It is noted that the non-uniformity of the light intensity distribution over the field-of-view of the image, caused by variation of the illumination, can be corrected by using an intensity distribution observed outside of the color sensitive temperature range of liquid crystals. For details see Fujisawa, et al. (1997). Likewise, errors caused by angular variation over the field-of-view can be accounted for by doing a calibration for each pixel.

The third calibration method we have considered is a three variable calibration technique with H, S, I that was implemented using the neural network shown in Fig. 5. It consists of three layers of neurons with a back propagation algorithm, similar in structure to that used by Kimura, et al. (1993) in R-G-B color space. Each of the variables H, S, I was given at the input layer, and the indicated temperature T_0 was produced at the output layer. The variables were connected to each other through a hidden layer having four units. The number of units in the hidden layer was varied in the course of the present study, and we found that four was the minimum number of units that produced a reasonable level of learning error in the neural network. In the learning process, the neural network modified the weights connecting each layer and the bias in order to minimize the error function $E=\sum(T_0-T)^2$, where T_0 is an output temperature of the neural network and T_m is the true temperature. The learning cycle of the neural network was performed 5000 times. We denote by T_c the final output of the neural net that is obtained after completing the learning process. Since this calibration method uses all three parameters of color; it is not necessary to deal directly with the problem of distinguishing low and high temperatures, as encountered in the calibrations with H and H/I. The neural net automatically accounts for this feature.

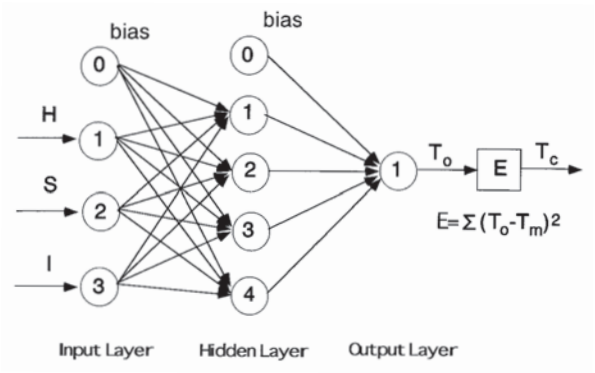

Fig. 5. Neural network model.

3.2 Calibration Errors

Figures 6(a)-(c) show the relationships between the calibrated temperature T_c and measured temperature T_m for the liquid crystals, where each of the three calibration techniques were applied: *H* calibration, *H*/*I* calibration and *H-S-I* neural network calibration, respectively. The error bars indicate calibration errors obtained from the differences between repeated experiments. Generally speaking, the calibration errors are smaller for the liquid crystal R32C2W than R29C4W, and they are roughly proportional to the temperature sensitive range. However, the magnitude of the errors depends on the calibration techniques. The errors increase gradually with the temperature for the *H* and *H*/*I* calibration, reflecting the decrease in temperature sensitivity of the *H* and *H*/*I* curves at higher temperatures. It can be seen that the calibration error is reduced in the *H*/*I* calibration in comparison with that of the *H* calibration. This is due to the difference in temperature sensitivity of *H* and *H*/*I* at higher temperatures. On the other hand, the calibration errors in the *H-S-I* neural network model are rather uniform over all the temperature range, and they are smaller than the maximum errors in *H*/*I* calibration. But, it should be kept in mind that the mean of the calibrated temperature itself deviates slightly from the measured temperature, due to the difficulty of minimizing the error in the neural network model. When increased learning times were used in an effort to create a smoother calibration curve, the error in the neural network model was increased locally by the problem of over-learning, especially at the low-end and the high-end of the temperature range. Therefore, the total calibration error in the neural network model is comparable to the maximum error in the hue/intensity calibration.

If one compares the temperature ranges over which the *H* and *H*/*I* calibrations yield the same error as the neural network, approximately ±0.2°C, the temperature ranges of the *H*/*I* method and the *H-S-I* neural network method are both substantially wider than that of the *H* calibration : 3.7°C and 5°C, respectively, versus 2.2°C (for R29C4W). The ranges were increased because the variable *H*/*I* is more sensitive at the high temperature end, and the neural network extends the calibrated temperature range below the minimum value at which the calibrations by *H* and *H*/*I* can be applied. In particular, given comparable errors, the temperature range of the *H-S-I* neural network method is more than double that of the hue calibration method.

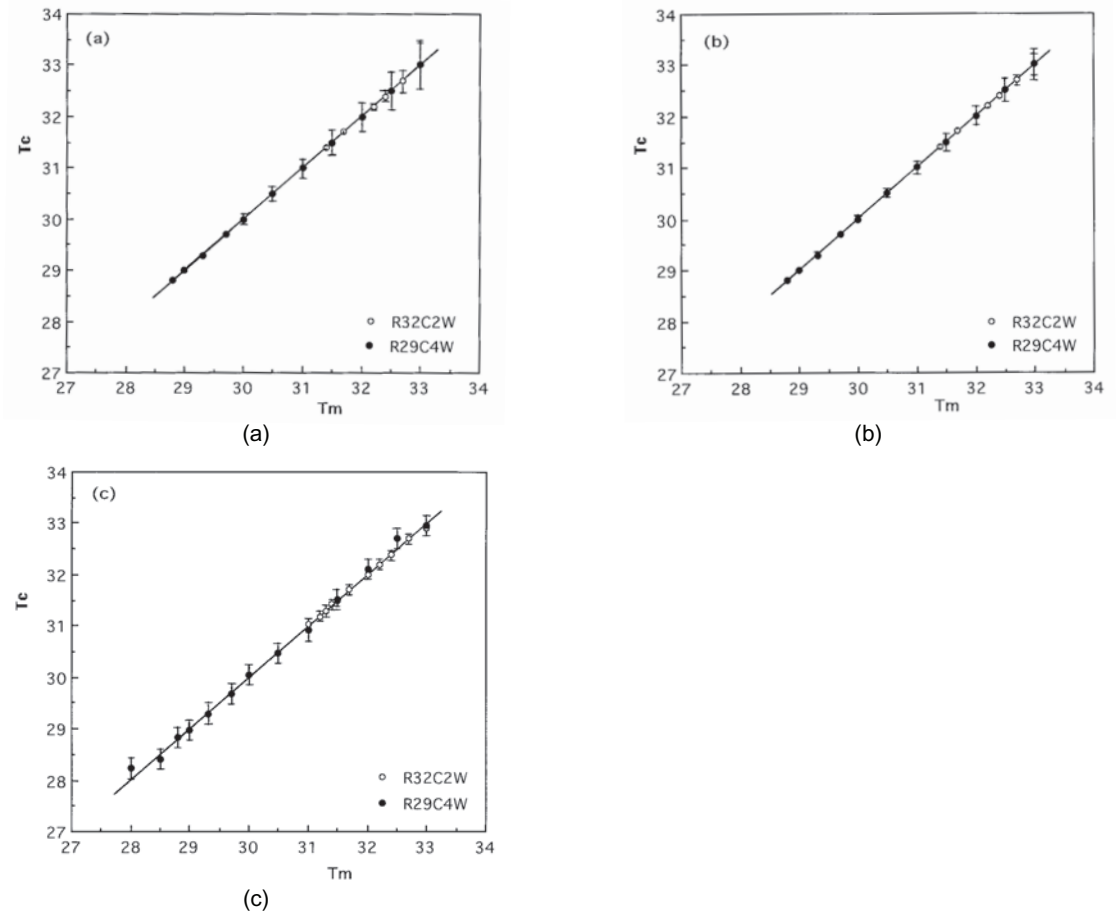

Fig. 6. Calibration errors. (a) *H* calibration, (b) *H*/*I* calibration, (c) *H-S-I* neural network.

3.3 Thermal Convection Over a Smooth Surface

Figure 7 shows a typical color image of thermal convection over a smooth surface visualized by illuminating an x-z plane. In the present experiments, the liquid crystal with smaller temperature range (R32C2W) was used to obtain better temperature resolution. The origin of the vertical coordinate z was located at the bottom boundary, and the center of the smooth surface was set to x=60mm, y=24mm and z=0mm. Several thermal plumes were generated from the bottom boundary, and they were visible in the form of high temperature areas of dark blue color. The surrounding low temperature fluid appeared green and brown. It was observed that the plume structures were generated randomly in space over the smooth surface and meandered across the fluid layer under the action of their buoyancy force. Most of the thermals convected within the lower half of the fluid layer, and they lost most of their excess heat during this upward motion. Only the large thermals, which were not diffused, reached the top surface and stayed there for a while.

Figure 8 shows a typical two-dimensional temperature distribution in the x-z plane at y=24mm. The color of the liquid crystal has been converted to temperature by means of the H/I calibration, but the resulting

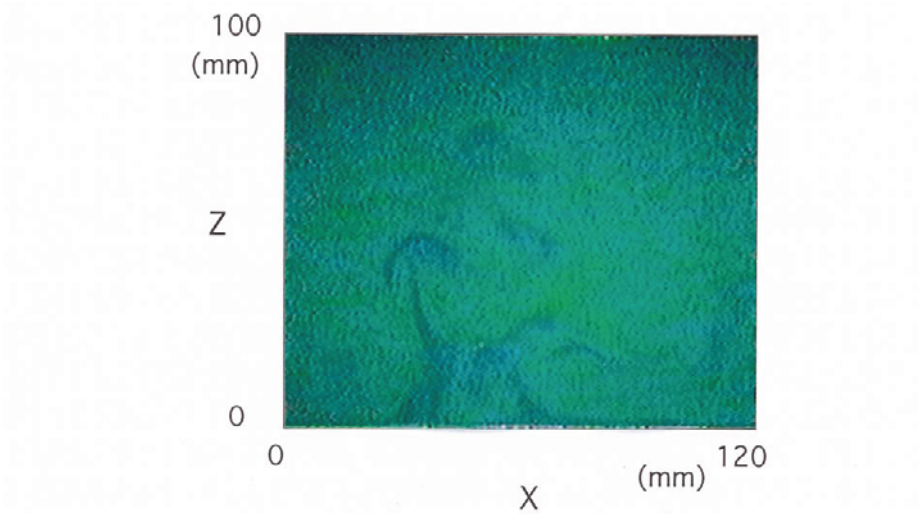

Fig. 7. Example of color image visualized by liquid crystal.

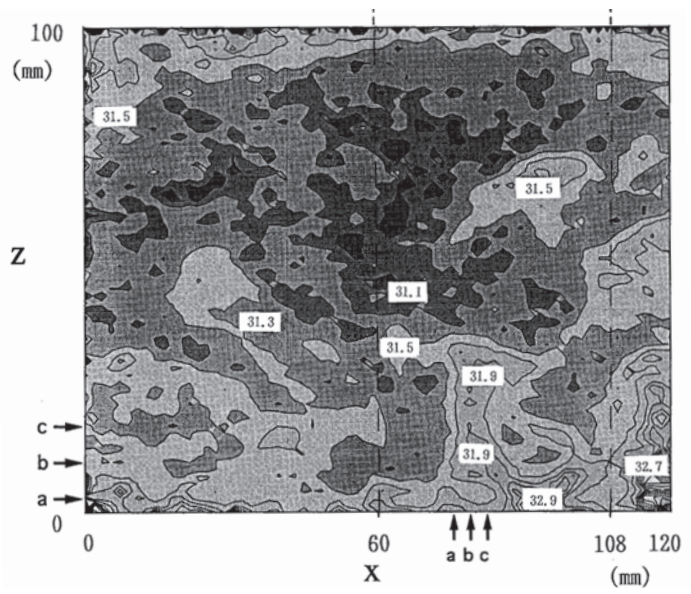

Fig. 8. Temperature distribution of thermal convection in the x-z plane at y =24mm (Unit in °C).

distribution agrees well with those found by the *H* and *H-S-I* calibration techniques. The gray scales indicate isothermal contour areas having a temperature range of 0.2°C, and the temperatures are labeled at various locations in the figure. The temperature contours of the thermal plumes are more clearly observed in this quantitative result than in the visualized color image, indicating the effectiveness of the color-to-temperature conversion. It is seen clearly that the thermal plumes generated from the heated surface had a high temperature region inside the plume and that the highest temperature appeared near the surface. More detailed structure of the thermal plumes will be presented below, where various sections of the three-dimensional temperature field of the plumes are reconstructed from the sliced two-dimensional images obtained by scanning the light sheet.

Figure 9 shows the temperature distributions in the vertical (*x*-*z* plane) at three *y*- positions centered on the plume structure that occurred around *x*=75~82mm in Fig. 8. Figure 10 shows temperature in corresponding *y*-*z* planes at various *x*- positions. In general, the fluid temperature was higher near the heating surface and decreases gradually with distance above the wall, as expected from existing data on the mean temperature (Adrian, et al.,

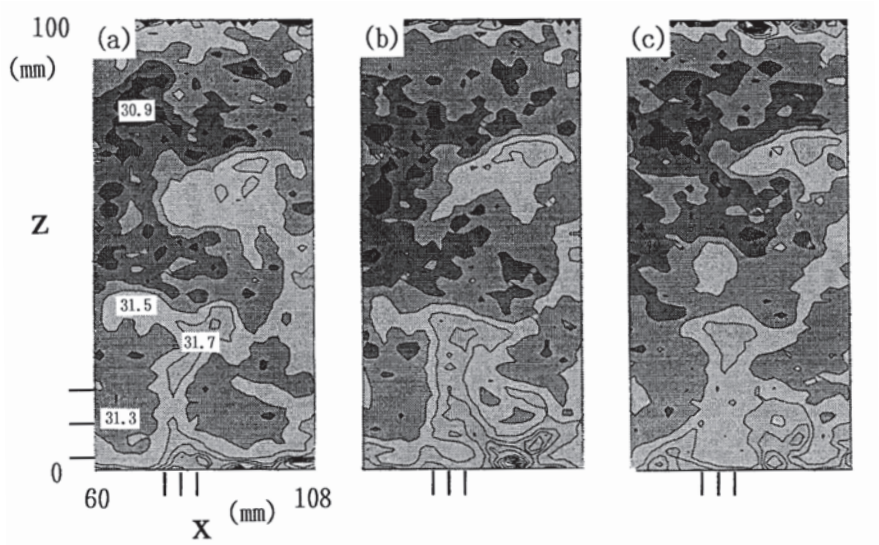

Fig. 9. Vertical cross-sectional distributions of temperature in thermal convection over smooth surface in the *x*-*z* plane (Unit in °C). (a) *y* =20mm, (b) *y* =24mm, (c) *y* =28mm.

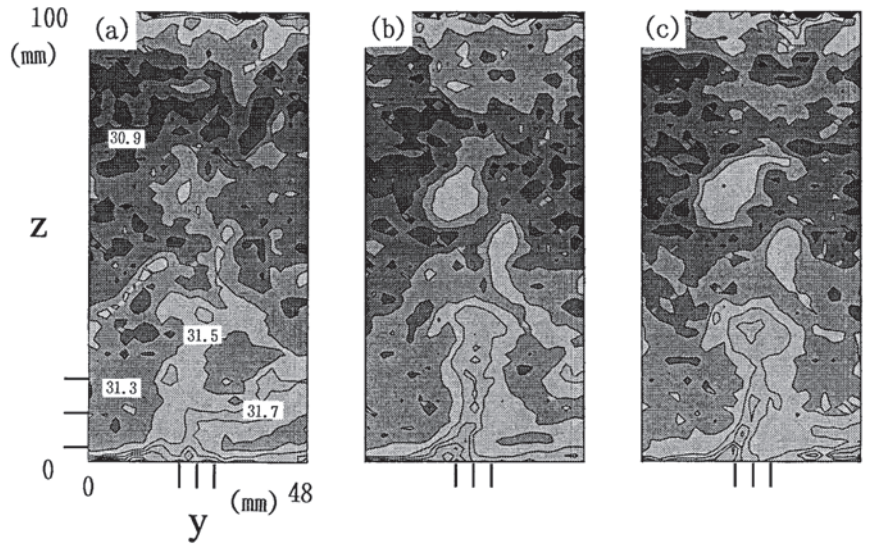

Fig. 10. Vertical cross-sectional distributions of temperature in thermal convection over smooth surface in the *y*-*z* plane (Unit in °C). (a) *x* =75mm, (b) *x* =79mm, (c) *x* =82mm.

1986, Balachandar, 1992, Koschmieder, 1993). But, each instantaneous temperature profile showed distinct thermal plumes having a mushroom structure. It was noticed that the temperature contour lines over the smooth surface varied substantially along the surface, reflecting the presence of near-wall turbulent structure. However, it should be mentioned that there is skewing of the thermal structure in y direction, of order 14mm, which is produced by the limited scanning time of the light sheet for the present experiment.

The patterns of the temperature field in thermal convection are of considerable interest (Gluckman et al., 1993). Figure 11 shows the temperature distributions at various horizontal cross-sections in the x-y plane. These data were found by composing the data from all of the x-z plane measurements. Such secions are normally very difficult to obtain in thermal convection experiments because the view of the horizontal x-y plane is blocked by the non-transparent upper and lower boundaries. Figure 11(a) clearly reveals the presence of a "spoke" pattern near the smooth surface, as has been observed by Willis and Deardorff (1974) and Schmidt and Schumann (1989). In this pattern, hot, buoyant fluid is accumulated in long thin ridges that lie on the lower surface, and sometimes intersect with each other. Thermals originate from these ridges, and they are often strongest at the points of intersection where the buoyancy forces of two or more ridges combine. Arrows in Fig. 11 (a) indicate these points. It should be mentioned that the plume structure in Figs. 9 and 10 develops from a high temperature area where the line structure intersects at x=93mm, y=24mm in Fig. 11 (a). It is expected that the small thermals move along the line structure and come together to the intersections to grow into larger, stronger plumes.

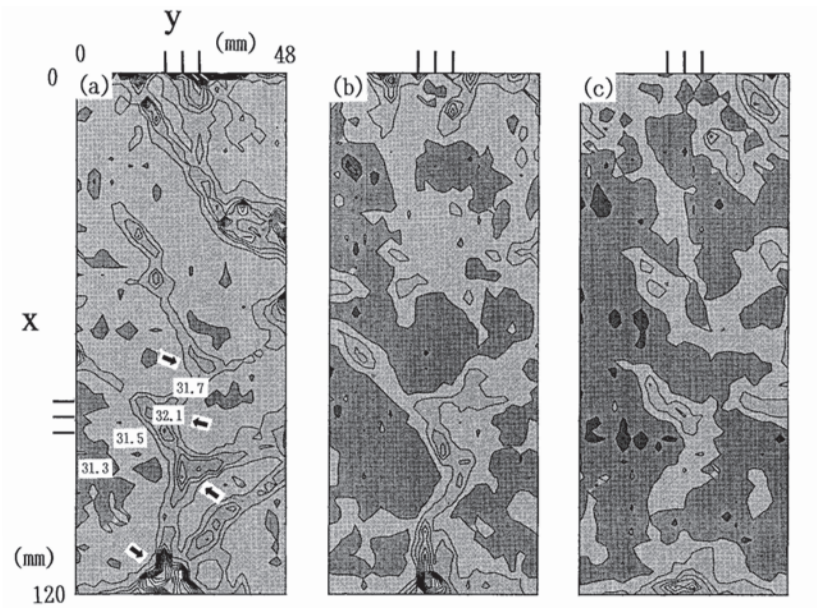

Fig. 11. Horizontal cross-sectional distributions of temperature in thermal convection over smooth surface in the x-y plane (Unit in °C). (a) z =3mm, (b) z =10mm, (c) z =18mm.

4. Conclusions

Three-dimensional measurements of temperature distributions in thermal convection have been carried out by scanning liquid crystal thermometry. The color of the liquid crystals is calibrated against temperature using various measurement variables derived from the primary R-G-B outputs of a color CCD: hue, hue/intensity and hue-saturation-intensity analyzed by a neural network calibration technique. The calibration technique with hue/intensity is effective for increasing the sensitivity and thereby extending the temperature range, but the measurable temperature range can be extended the most by the H-S-I neural network (to more than twice the range of the hue calibration). Scanning liquid crystal thermometry combined with the extended range hue/intensity calibration was successfully applied to the three-dimensional temperature measurement of turbulent thermal convection over smooth surfaces. The measurements captured, in three dimensions, many aspects of the thermal structure that are known to occur in turbulent convection over a smooth, heated surface.

Acknowledgments

The authors would like to thank Dr. R. D. Keane of University of Illinois for his advice in the experiments, and also Mr. T. Matsuura and Mr. Nakabayashi of Gunma University for their help in developing the neural network calibration technique. The research was supported in part by U.S. National Science Foundation Grant ATM95-22662.

References

Adrian, R. J., Ferreira, R. T. D. S., Boberg, T., Turbulent Thermal Convection in Wide Horizontal Fluid Layers, Exp. Fluids, Vo l.4, (1986), 121-141.

Akino, N., Kunugi, T., Ichimiya, K., Mistushiro, K., Ueda, M. Improved Liquid-Crystal Thermometry Excluding Human Color Sensati on. (Part 1: Concept and Calibration), ASME Heat Transfer Div., Vol. 58, (1986), 57-62.

Akino, N., Kunugi, T., Ueda, M., Kurosawa, A., Liquid Crystal Thermometry Based on Automatic Color Evaluation and Applications to Measure Turbulent Heat Transfer, in Transport Phenomena in Turbulent Flows, (1988), 807-820.

Balachandar, S., Structure in Turbulent Thermal Convection, Phys. Fluids, Vol. 4, (1992), 2715-2726.

Dabiri, D. and Gharib, M., Digital Particle Image Thermometry (The Method and Implementation), Exp. Fluids, Vol. 11, (1991), 77-86.

Fujisawa, N., Adrian, R. J. and Keane, R. D., Three-Dimensional Temperature Measurement in Turbulent Thermal Convection Over Sm ooth and Rough Surfaces by Scanning Liquid Crystal Thermometry, Proc. Intl. Conf. Fluid Engr., Tokyo, Japan, (1997) , 1037-1042.

Gluckman, B. J., Willaime H., Gollub, J. P., Geometry of Isothermal and Isoconcentration Surfaces in Thermal Turbulence, Phys. Fluids, Vol. A5, (1993), 647-661.

Hallcrest, Inc., (1996) Private communication.

Kasagi, N., Moffat, R. J., Hirata, M., Liquid Crystals, In Handbook of Flow Visualization, (Ed. Yang, W.J.), (1989), 105-124, N ew York, Hemisphere.

Keane, R. D. and Adrian, R. J., A Qualitative Study of Unsteady Non-Penetrative Thermal Convection from Non-Uniform Surfaces, 1 2th Australasian Fluid Mech Conf, Sydney, Australia, (1995), 1-4.

Keane, R. D., Fujisawa, N. and Adrian, R. J., Unsteady Non-Penetrative Thermal Convection from Non-Uniform Surfaces, TAM Report No.847 UIUC-ENG-97-6008, (1997), 1-26.

Kimura, I., Takamori, T., Ozawa, M., Takenaka, M. and Manabe, Y., Quantitative Thermal Flow Visualization Using Color Image Pro cessing (Application to a Natural Convection Visualized by Liquid Crystals), ASME-FED 85, Flow Visualization (Eds Khalighi, B, Braun, M .J. and Freitas, C.J.), (1989), 69-76.

Kimura, I., Kuroe, Y., Ozawa, M., Application of Neural Networks to Quantitative Flow Visualization, J. Flow Visualization and Image Processing", Vol. 1, (1993), 261-269.

Kobayashi, T., Saga, T. and Doh, D. A Three-Dimensional Simultaneous Scalar and Vector Tracking Method, Proc. Intl. Workshop on PIV, Fukui, Japan, (1995), 33-43.

Koschmieder, E. L., Benard Cells and Taylor Vortices, Cambridge University Press, (1993), 193.

Nozaki, T., Mochizuki, T., Kaji, N. and Mori, Y. H., Application of Liquid-Crystal Thermometry to Drop Temperature Measurements , Exp. Fluids, Vol. 18, (1995), 137-144.

Ozawa, M., Muller, U., Kimura, I. and Takamori, T., Flow and Temperature Measurement of Natural Convection in a Hele-Shaw Cell Using a Thermo-Sensitive Liquid-Crystal Tracer, Exp. Fluids, Vol. 12, (1992), 213-222.

Rhee, H. S., Koseff, J. R. and Street, R. L., Flow Visualization of a Recirculating Flow by Rheoscopic Liquid and Liquid Crystal Techniques, Exp. Fluids Vol. 2, (1984), 57-64.

Schmidt, H. and Schumann, U., Coherent Structure of the Convective Boundary Layer Derived From Large-Eddy Simulations, J. Flui d Mech., Vol. 200, (1989), 511-562.

Wilcox, N. A., Watson, A.T. and Tatterson, G.B., Color/Temperature Calibrations for Temperature Sensitive Tracer Particles, Pro c. Intl. Symp. Physical and Numerical Flow Visualization, Albuquerque, USA, (1985), 65-74.

Willis, G. E. and Deardorff, J.W., A Laboratory Model of the Unstable Planetary Boundary Layer, J. Atmos. Sci ., Vol. 31, (1974), 1297-1307.

Authors' Profiles

Nobuyuki Fujisawa: He was educated at Iwate University (B.E. 1977) and at Tohoku University (M.E. 1979, D.E. 1983) in Japan. He joined to Gunma University in 1983 and worked as a research scientist in the field of turbomachinery, turbulence modelling and flow visualization. Later he promoted to an associate professor in mechatronics division in 1991 and he extended his research field to active control of flow-induced vibration and flow imaging. Since 1997, he has been a professor of Niigata University and continuing the research in active control of flow and flow-induced noise, flow visualization and image processing and PIV in thermal and fluid phenomena.

Ronald J. Adrian: He was educated at the University of Minnesota in mechanical engineering (B.M.E. 1967, M.S. 1969) and at Cambridge University in physics (Ph.D, 1972). His research interests are the space-time structure of turbulent fluid motion and the development of techniques, both experimental and mathematical, to explore this structure. Methods to which he has made fundamental contributions are the laser Doppler velocimeter technique, the method of particle image velocimetery and the stochastic estimation method. He is the Hoeft Prof. of Engineering at the University of Illinois, Urbana-Champaign, and Director of the Laboratory for Turbulence and Complex Flow in the Department of Theoretical and Applied Mechanics.